POLITECNICO DI TORINO

International Master in Physics of Complex Systems

Politecnico di Torino

UNIVERSITÉ FRANCO ITALIENNE | UNIVERSITÀ ITALO FRANCESE

Institut de Neurosciences des Systèmes

Tesi di laurea magistrale

Mean field derivation for a network of spiking neurons with dopamine modulation

Supervisor
Prof. Alessandro Pelizzola, DISAT
Damien Depannemaecker, INS

Candidate
Gabriele Casagrande

Academic year 2023/2024

One of the main challenge in neuroscience is to model the behaviour of the brain at different scales, both in physiological and pathological conditions. However, the inherent complexity of the brain make it really challenging to tackle the problem of studying the underlying brain dynamics directly. In an attempt to ease this challenge several techniques borrowed from physics have been exploited.

One of these approach consist into derive the macroscopic dynamics of a population of neurons through mean field approximations, which can be approached in different way [1, 2, 3, 4, 5, 6, 7]. These models are based on the idea that, given the large number of neuron in a single population, we can focus our attention into describing the average activity of the group, instead that of each individual component. In this way one could explore the emergence of collective behaviour which are not present at single level.

In this work we exploit the mean field derivation framework presented by [1, 2] to achieve a system of closed equations for a network of adaptive quadratic integrate-and-fire (aQIF) neurons [8]. The quadratic integrate-and-fire (QIF) is one of the most used model in the context of theoretical neuroscience. It describes the evolution of the membrane voltage as a quadratic differential equation, imposing a certain threshold value. Once this value is reached the neuron fires a spike and the membrane voltage value is reset to a fixed value.

The aQIF model represents an extension of this model in which a second variable, slower than the membrane voltage, describes the adaptation dynamics. This allows the system to exhibit a wider variety of dynamical behaviour (as synchronous bursting) than the QIF model [8, 2].

We extend the aQIF [8] model, by explicitly considering the modulation effect due to the presence of dopamine in the extracellular space. Dopamine is a crucial neuromodulator that plays a pivotal role in several essential functions within the central nervous system, including regulation of movement, emotion, motivation, and reward [9, 10, 11]. In health, dopamine facilitates motor control, as exemplified by its action in the basal ganglia, and contributes to the pleasure and reinforcement mechanisms that drive learning and behavior [12, 13, 14]. Pathologically, dysregulation of dopamine levels is implicated in various disorders [15, 16]. For instance, Parkinson's disease is characterized by the degeneration of dopaminergic neurons in the substantia nigra, leading to motor deficits such as tremors and rigidity. Conversely, hyperactivity of dopaminergic pathways is associated with schizophrenia, contributing to symptoms such as hallucinations and delusions.

In the derivation, we first assume a population density approach [17], i.e. we consider the distribution of neurons over all possible states. Furthermore, we exploit the Lorentzian ansatz, whose validity for a network of Izhikevich neurons was demonstrated in previous works [1, 18]. In order to derive a finite set of equations we also exploit the first-order moment closure assumption presented in [19].

We confront the derived mean field set of equations with simulations of the related network of all-to-all coupled neurons to identify whether it is able to correctly reproduce the same dynamical features. Finally, we address some limitations of this procedure and how to possibly resolve them.

Contents

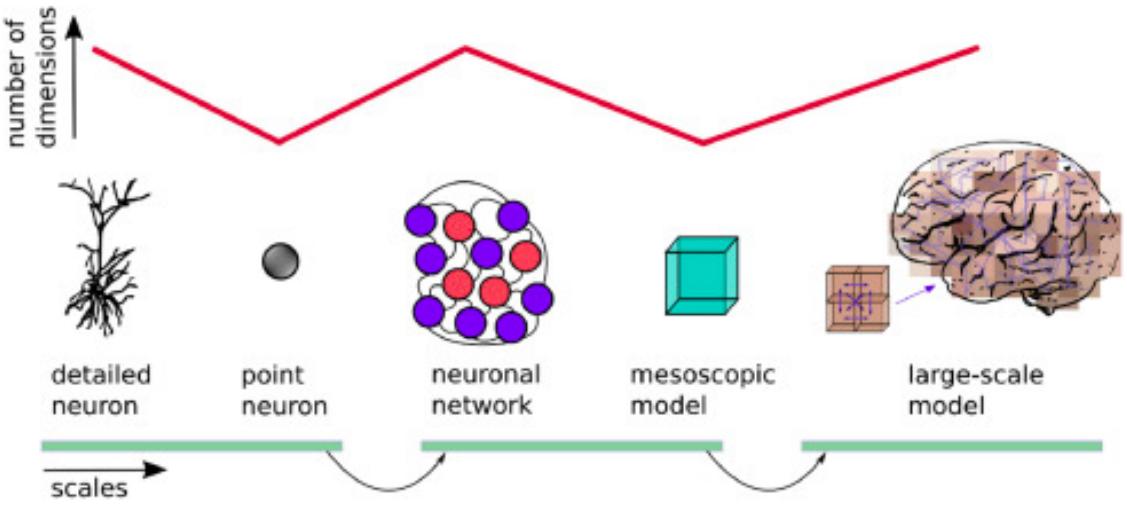

Figure 1: Illustration taken by [25] which highlight the different sales at which we can describe the problem of understanding brain activity.

1 Introduction

1.1 Modelling brain activity

Initially, first approach to modelling of the brain began in late 19th century and the beginning of the following one (Marcelle and Louis Lapicque, 1905). Later on, in 1952, Hodgkin and Huxley published their pioneristic experimental study about the biophysics mechanism behind the functioning of the squid giant axon [20]. This studies were fundamental to answer a set of "practical" questions which allows to understand the mechanism through which a single neuron is activated, i.e. the concept of action potential. However, the brain functions span across multiple scales: cellular (or even molecular) phenomena, large-scale networks until arriving to social interactions between individuals. Thus, it is of fundamental importance to address the problem of this multiscale organization in order to unreveal the variegate dynamical repertoire of brain activities, which held the bases for complex behaviors that characterize this fascinating organ.
In this particular work we will try describe a method which allow to build a bridge between the microscopic description of a single neuron and the behavior of population of heterogeneous neurons, using multi-scale brain modelling. At microscale, models are characterized by the description of variables which define neurons and synapses. This phenomena can be analyzed experimentally using various techniques that can unveil for example intracellular membrane potential and ion concentration changes. This knowledge allows biophysically accurate single neuron model, described by few parameters that can be derived from experimental recordings. By linking together several of these models one is able to generate accurate microcircuits that retain a fine representation of the dynamics of local networks [21, 22].
However, due to the impressive high number of single elements required to effectively finely describe these circuits, the practical difficulties of their implementation grows very rapidly. Hence, they need to be simplified into point neurons model to allow the possibility of performing simulations and analyses of spiking neuron models (SNNs) [23].
Nonetheless, also SNNs models can quickly become inefficient due to the high number of single components so that one can consider to summarizes their important statistical properties into macroscopic models that represent the average activity of a population of neurons.
There exist several techniques to perform the passage from microscopic to macroscopic scale [24, 25], one of these consists into exploit mean field theory. By developing this theory we aim to extract typical behavior that characterizes neural circuits, in the sense that they do not depend on microscopic properties of individual neurons (as long as their number is large).
Finally, we can consider a further scale of integration by going to whole-brain models. They are made by nodes connected by edges that reproduce the different brain functional areas. Each node contains one of the simplified model of the neuron activity by mentioned before (e.g. mean-field, neural masses). Those models are usually

supported by whole-brain recordings obtained with different techniques, e.g., MRI, EEG, EMG, PET [26].

1.2 Adaptive integrate-and-fire model (aQIF)

In the following we will describe a mean field reduction techniques developed by Chen and Campbell [2] which exploit several concepts coming from statistical physics (e.g, population density approach, moment closure, Lorentzian ansatz) allow to derive a macroscopic reduction of a population of neurons.
The starting point is the microscopic description of a single element of this population. Here, we consider the widely used single-neuron model proposed by Izhikevich [8], also known as the adaptive quadratic integrate-and-fire (aQIF) model.
Each neuron is described by a 2D system of ordinary differential equations for the membrane potential v(t) and the adaptation current u(t):

$$v_i' = av_i^2 + bv_i + c - u_i + I_{ext} \tag{1}$$
$$u_i' = \alpha(\beta v_i - u_i) \tag{2}$$

with $i = 1, 2, \ldots, N$. The time derivation is identified with the notation $' = d/dt$.
The adaptation variable u provides a negative feedback to the growth of v and it accounts for various mechanisms that are involved in the dynamics of the membrane potential, i.e. the activation of K+ ionic currents and inactivation of Na+ ionic currents.
The parameter α describes the time scale of the recovery variable u, the smaller is its value the slower is the recovery. Instead, β represents the sensitivity of the recovery variable u to the sub-threshold fluctuations of the membrane potential v. The external common current is described by I_{ext}.
The insertion of the adaptation variable is fundamental, because it allows the possibility to obtain several dynamical regimes which are not present in the simpler quadratic integrate-and-fire (QIF) model, where just the membrane potential were considered.
When the membrane potential crosses the threshold (i.e an action potential is emitted) the following reset condition applies:

$$\begin{aligned} v_i \geq v_{peak}, \text{ then } v_i &\leftarrow v_{reset} \\ u_i &\leftarrow u_i + u_{jump} \end{aligned} \tag{3}$$

Here, v_{reset} is the after-spike reset value of the membrane potential v while u_{jump} explains the after-spike jump caused by slow high-threshold conductance.
Various choices of the parameters result in various intrinsic firing patterns, as can be observed in 2.

In addition to that, we considered two extra-terms in the evolution equation of the membrane potential. The first one is a random variable, η_i, drawn according to a distribution $\mathcal{L}(\eta)$ defined on $(-\infty, \infty)$, which represents an intrinsic current and allows to define an heterogeneity between the different neurons within the same population [1, 2].
Furthermore, neurons are connected through the following model for synaptic interactions I_{syn}, which takes into account a modulation effect as we will point out later.

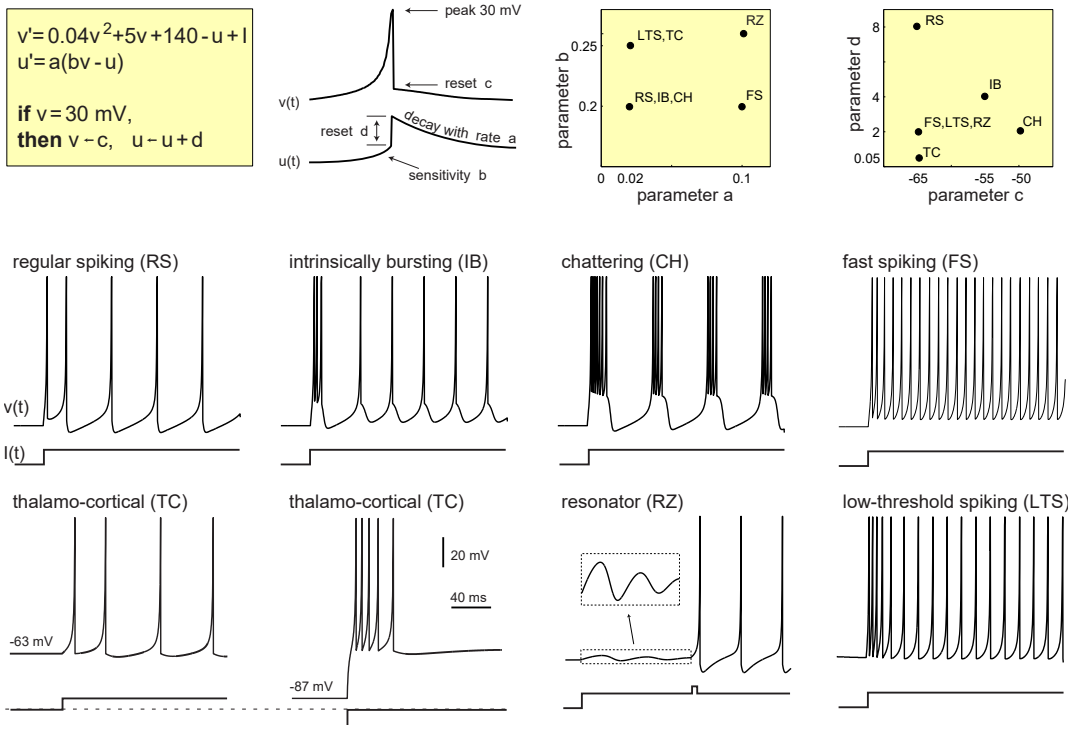

Figure 2: Representation of different dynamical behavior associated to different type of known neurons [8]. Distinct regimes are obtained by changing the values of parameters that define the model. Electronic version of the figure and reproduction permissions are freely available at www.izhikevich.com .

1.3 Neuromodulation

Living beings are constantly subjected to a huge variety of stimulus. Depending on both the external and internal conditions in which it is perceived, it leads to different reactions. However, organism only has s finite number of neuronal circuit, hence each of them must account for more than a single function. Here it is neuromodulation comes into play, allowing changes in the function of sensory circuits without changing their 'fixed structure' [27, 28].

Studies about this topic are mostly interested in how to alterate, electrically or chemically, the activity in different areas of nervous system with the aim of obtaining therapeutic results. One of the main strength of neuromodulation is its characteristic of being non-destructive, reversible, and adjustable, so that it can be applied in a variety of treatments [29, 30].

Nowadays, technologies and therapies involving neuromodulation are developed in many clinical areas to treat a wide range of pathology, that include for example disorders of cardiac pacing, epilepsy and psychiatric and neurobehavioral disorders [31, 32, 33, 31, 34].

In the following, we will mainly interested in how chemical modulation shapes brain dynamics. In this context the modulation effect is normally initiated by the binding of a molecule, called neuromodulator, to specific receptors. This process causes a cascade of reactions that lead to changes in dynamical behavior (firing rate or bursting properties) or the shape of the action potential [35].

Moreover, neuromodulators also operate at a larger scale, affecting coordination and interplay between distinct connected neural networks. As a a consequence, as we previously mentioned, they are responsible for changes in cognitive and behavioural processes [36, 37]. Thus, in order to fully understand the function of a certain neuromodulator within the complex behavior of brain both in physiological and altered state, it is important to understand both its biophysical mechanism and the effect it induces in the behavior of the neural dynamics.

Common neuromodulators are serotonin, dopamine, histamine and norepinephrine. In the current work, we mostly focused on the effect of dopamine, which is involved in several processes, both in health and disease.

Dopamine is endogenously produced in small regions of densely packed neurons (mostly in the ventral tegmental area and substantia nigra pars compacta). Afterwards these neurons project this modulator to targeted brain regions [38]. Dopaminergetic effects are related to reward reward processing [39]. Moreover, it is also associated

with to cognitive processes and behaviors such as working memory, response to novelty or adverse stimuli [13] and cognitive control [40]. In this context dopamine was shown to be fundamental to perform task that require an effort [11].
Dysfunction in dopamine regulation, and neuromodulator more in general, was correlated to the presence of several disorders [41], for instance schizofrenia and Parkinson's disease. Dopamine regulation disruption have also been related to addiction, where the consumption of drug is insanely related to reward and satisfaction causing a reinforcement in the need for consumption [31]. Finally, dopaminergic modulation related cognitive performances, was observe to change as a consequence of aging [42].

2 Methods and Results

2.1 Spiking network model

In this section we are gonna present the mean field procedure which allowed us to derive a reduced system to describe the behavior of a spiking network of neurons.
First of all, starting from the equations described in , we added an additional term to the evolution of membrane potential in order to take into account the effect of neuromodulation.
Namely, we consider that neurons are connected through the following model for synaptic interactions, which takes into account a modulation effect M_{D1} due to the presence of D1-type dopamine receptors:

$$I_{syn} = (M_{D1} + B_{M_{D1}})g_a s_{a,i}(e_a - v_i) + g_g s_{g,i}(e_g - v_i), \tag{4}$$

where $g_{a,g}$ and $e_{a,g}$ are the maximum synaptic conductance and the reversal potential respectively for the excitatory (AMPA) and inhibitory (GABA) synapses.
The variables $s_{a,i}$ and $s_{g,i}$, both $\in (0,1)$, represent the synaptic activation, i.e. the portion of open ion channels in post-synaptic neurons due to the action of pre-synaptic ones.
We assume the network to be all-to-all coupled (as in previous works [1, 2]) so that each neuron receives the summed output of all the pre-synaptic ones. As a consequence both $s_{a,i}$ and $s_{g,i}$ are homogeneous across all the neurons, hence we refer at them as s_a and $s_g, \forall i \in (1, N)$.
In this work we focus on a network only composed by an excitatory population of all-to-all coupled neurons.
Additional inputs, both excitatory and inhibitory, will be included by moving to neural mass scale, where we will consider multiple interacting populations of neurons.
Concerning the time evolution of the synaptic gating variables, we consider the single exponential synapse transmission for the evolution of the excitatory synaptic dynamics and an exponential decay for the inhibitory one. We point out that this choice is made because we consider the example of a single excitatory population of all-to-all connected neurons. Nevertheless, it would be possible to also have 2 populations, both excitatory and inhibitory. In the latter case we would have also the sum of all the inhibitory inputs on the inhibitory population. For the specific case we consider, the evolution equations for the synaptic activation reads:

$$\begin{cases} s_a' = -s_a/\tau_{s_a} + \frac{s_{j,a}}{N}\sum_{i=1}^{N}\sum_{t_i^k<t}\delta(t - t_i^k) \\ s_g' = -s_g/\tau_{s_g} \end{cases} \tag{5}$$

Here, t_i^k is the time of the $k-th$ spike of neuron i and $\delta(t)$ is the Dirac delta function.
We point out that also the alpha function synapse and the double exponential synapse could be considered [43] for describing the synaptic activation variable. However, they are described by a system of two coupled ordinary differential equations, adding an additional term to the final system. Thus, in the following, we stick to the model 5 for simplicity.
The modulation effect of dopamine receptors M_{D1} presented in 4, is described by an exponential decrease and a sigmoid-shaped function [44], which represent the proportion of receptors activated as a function of the external dopamine concentration $[Dp]$:

$$\tau_{M_{D1}} M_{D1}' = -M_{D1} + \frac{R_d}{1 + exp(S_p([Dp] + 1))} \tag{6}$$

Here, R_p represents the receptor density in a given population, while S_p is a parameter that corresponds to the sensitivity of receptors to variation in extracellular dopamine concentration. The sign of S_p indicates whether the receptors will be activated ($S_p > 0$) or reduced ($S_p < 0$) by the presence of dopamine. Its absolute value indicates the strength of this effect, hence the more $|S_p|$ is increased the more receptors are activated ($S_p > 0$) or reduced ($S_p < 0$) with the same value of external dopamine concentration 3. Interestingly, neuromodulation effects are usually related to increase in the sensitivity of receptors to their characteristic stimulus.
As mentioned before, the term $[Dp]$ represents the concentration of dopamine molecules in the extracellular space, and its variation in time is described by:

$$\tau_{[Dp]}[Dp]' = kc_{dopa} - \frac{V_{max} + [Dp]}{K_m + [Dp]} \tag{7}$$

The first term accounts for the increase due to the presence of projection from dopaminergic neurons, through c_{dopa}, scaled by a factor k different for each region, whereas the second is the general form of the Michaelis-Menten equation [44].

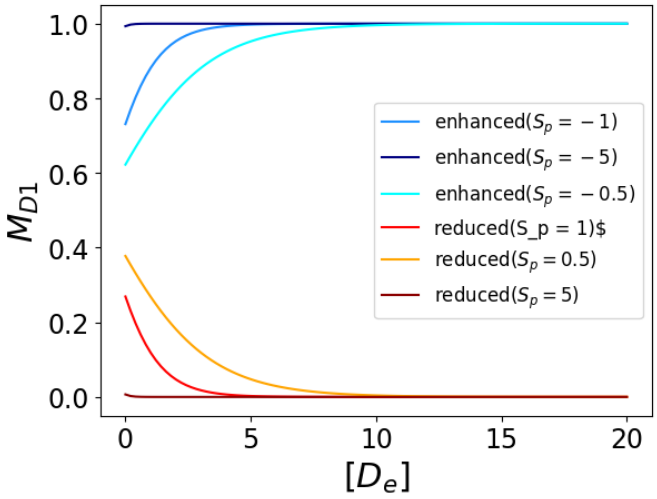

Figure 3: Effect of sensitivity S_p on the dynamics of M_{D1} as the concentration of dopamine $[Dp]$ changes. Parameter used for simulation, apart of S_p, are reported in 1. We may notice that regarding whether the receptor activity is enhanced or reduced by the presence of dopamine, M_{D1} evolves with different speed toward a stable fixed point which depends on the nature of S_p.

2.2 Mean field reduction for spiking neural network

In this section, we are going to derive a low-dimensional mean model to approximate the behavior of the full population of neurons described in 2.1, with the addition of the synaptic current I_{syn} and the related terms presented in the previously in 576. In particular, we consider to be in the thermodynamic limit, i.e. $N \to \infty$.
The first step consists of considering a population density approach for the network of neurons [19] by defining $\rho(t, v, u, \eta)$, which represents the density of neurons at position (v, u) in the phase space, with a certain value η for the intrinsic current. It is important to know that we assume the variation in dopamine concentration and its receptors are much slower than the firing rate dynamics and therefore it doesn't affect the derivation of the mean field system.
Since the total number of neurons is assumed constant through the dynamics, the following continuity equation holds:

$$\frac{\partial \rho}{\partial t} + \nabla \cdot J(t, v, u, s, \eta, M_{D1}) = 0 \tag{8}$$

Where $J(t, v, u, s, \eta, M_{D1})$ is the probability flux and it is defined as [17, 19, 45]:

$$\begin{aligned} J = \begin{pmatrix} J^v \\ J^u \end{pmatrix} = \begin{pmatrix} G^v(v, u, \eta, s, M_{D1}) \\ G^u(v, u) \end{pmatrix} \rho(t, v, u, \eta) = \\ = \begin{pmatrix} av^2 + bv + c - u + I_{ext} + I_{syn} + \eta \\ \alpha(\beta v - u) \end{pmatrix} \rho(t, v, u, \eta) \end{aligned} \tag{9}$$

Moreover, taking into account the reset conditions 3, the following boundaries condition was defined:

$$J^v(v_{peak}, u) = J^v(v_{reset}, u_{jump} + u) \tag{10}$$

Moreover, we also assume that the flux is vanishing at the boundaries of u [19], meaning $J = 0$ as $u \to \pm\infty$. This is due to the fat that although $u \in (-\infty, \infty)$ the probability to observe high values of the absolute value $|u|$ decays fast toward 0, thus making the flux virtually vanishing at ∂u [43].
To describe the mean field behavior of the full system we define some useful macroscopic observables:

- the mean membrane potential, defined as the average over the entire population of neurons:

$$\langle v(t) \rangle = \int_{\partial \eta} \int_{\partial u} \int_{\partial v} v \rho(t, v, u, \eta) d\eta du dv \tag{11}$$

- the mean adaptation current over the full network:

$$\langle u(t) \rangle = \int_{\partial \eta} \int_{\partial u} \int_{\partial v} u \rho(t, v, u, \eta) d\eta du dv \tag{12}$$

- the population firing rate, namely the flux of neurons through v_{peak} over the whole range of u and η:

$$r(t) = \int_{\partial\eta}\int_{\partial u} J^v(t, v_{peak}, u, \eta, M_{D1}, s)d\eta du \tag{13}$$

Furthermore, we highlight that the flux at the threshold can be seen as the number of spikes fired by the network of neurons at a certain moment [43]. In this sense, the synaptic dynamics can be related to the population firing rate, in the limit $N \to \infty$, by the form:

$$s_a' = -\frac{s_a}{\tau_{s_a}} + s_{a,jump} r(t), \tag{14}$$

with $s_{a,jump}$ and τ_{s_a} equal for every excitatory synapse. A complete derivation of the above equation is described in 4.1.
Continuing with the derivation, we proceed to simplify the expression of the mean adaptation current derivative with respect to time by exploiting the definition of the continuity equation 8:

$$\langle u(t)\rangle' = \int_{\partial\eta}\int_{\partial u}\int_{\partial v} u\frac{\rho}{\partial t}d\eta du dv = -\int_{\partial\eta}\int_{\partial u}\int_{\partial v} u(\frac{\partial J^v}{\partial v} + \frac{\partial J^u}{\partial u})d\eta du dv \tag{15}$$

The integral above can be divided into two different terms which will be analyzed separately.
Consider the first one and proceed to integrate over ∂v:

$$\begin{aligned}\int u\left(\frac{\partial J^v}{\partial v}\right) dv du d\eta = \int uJ^v|_{\partial v} du d\eta \approx u_{jump}\int\left[(uJ^v)|_{\partial u} - \int J^v(v_{peak})dv\right] d\eta du = \\ = -u_{jump}\int J^v(v_{peak}) du d\eta\end{aligned} \tag{16}$$

In the second passage, we assume that $\langle u|\eta\rangle \gg u_{jump}$ and perform a Taylor expansion. This passage highlight the fact that this assumption consists into replace spike train for individual neuron with average firing rate $r(t)$. Afterward, we use the fact that the flux disappears at the boundaries of u.
The second term instead reads:

$$\int u\left(\frac{\partial J^u}{\partial u}\right) dv du d\eta = \int\left[(uJ^v)|_{\partial u} - \int J^u du\right] dv d\eta = -\langle G^u\rangle = -\alpha\left(\beta\langle v\rangle - \langle u\rangle\right) \tag{17}$$

Where, in the second step, we consider once again the disappearance of the flux at the boundary of u, together with the definition of mean value, since $J^u = G^u\rho(v, u, \eta)$, and its linearity.
Combining the two results the following expression for the evolution of the mean adaptation current is found:

$$\langle u(t)\rangle' = \alpha(\beta\langle v\rangle - \langle u\rangle) + u_{jump} r(t) \tag{18}$$

Moving forward in the derivation, we exploit the population density approach to simplify the expression of the remaining observables as done in previous works [17, 43, 46].
To achieve that, we decompose the probability density function in the following conditional form:

$$\rho(v, u, \eta) = \rho^u(u|v, \eta)\rho^v(v|\eta)\mathcal{L}(\eta) \tag{19}$$

As a consequence of the above decomposition, we can redefine the mean membrane potential and the population firing rate, by integrating over u.
Hence, for the first one, we obtain:

$$\langle v(t)\rangle = \int_{\partial\eta}\int_{\partial v}\int_{\partial u} v\rho^u(t, u|v, \eta)\rho^v(t, v|\eta)\mathcal{L}(\eta)dv du d\eta = \int_{\partial\eta}\mathcal{L}(\eta)d\eta\int_{\partial v} v\rho^v(t, v|\eta), \tag{20}$$

Where we exploit the normalization condition on the marginal density $\rho^u(u|v, \eta)$.
Similarly, the population firing rate became:

$$\begin{aligned} r(t) = \int_{\partial\eta}\int_{\partial u} G^v(v_{peak}, u, \eta)\rho^u(t, u|v, \eta)\rho^v(t, v|\eta)\mathcal{L}(\eta)d\eta du = \\ = \int_{\partial\eta}\rho^v(t, v|\eta)\mathcal{L}(\eta)d\eta G^v(v_{peak}, \langle u|v, \eta\rangle, \eta) = \int_{\partial\eta}\rho^v(t, v|\eta)\mathcal{L}(\eta)d\eta G^v(v_{peak}, \langle u|\eta\rangle, \eta)\end{aligned} \tag{21}$$

It is important to note that in the last step, we used the first-order moment closure assumption $\langle u|v,\eta\rangle = \langle u|\eta\rangle$, taking inspiration from the previous works[19, 46].
This means that u_i is sensitive to $\langle v(t)\rangle$ but not on a single value of v_i. The validity of this assumption is supported by numerical simulations [43]. In addition, by integrating the continuity equation over the adaptation current u, we end up with a continuity equation for $\rho^v(t,v|\eta)$, describing its evolution in time:

$$\frac{\partial}{\partial t}\rho^v(t,v|\eta) = -\frac{\partial}{\partial v}\left[G^v(v,\langle u|\eta\rangle,\eta,M_{D1},s)\rho^v(t,v|\eta)\right] \tag{22}$$

Notice that in the last step, the first-order moment closure assumption is used once again.
Both $\langle v(t)\rangle$ and $r(t)$ depend on $\rho^v(t,v|\eta)$, hence to simplify further the mean field equations we proceed into making an ansatz for the functional form of the probability distribution of the voltage membrane.
We now exploit the fact that 22 has a Lorentzian shaped stationary solution and we assume that $\rho^v(t,v|\eta)$ follows a distribution of the same functional form in time [1, 2, 18], leading to the following ansatz:

$$\rho^v(t,v|\eta) = \frac{1}{\pi}\frac{x(t,\eta)}{\left[v-y(t,\eta)\right]^2 + x^2(t,\eta)}, \tag{23}$$

with $x(t,\eta)$ and $y(t,\eta)$ respectively the half-width at half-maximum and the location of the center of the distribution.
Taking into account this expression for the conditional density function one can also rewrite the observables defined above in term of the parameter of the Lorentzian distribution.
First, since the Lorentzian distribution has mean only in principal value sense, $y(t)$ is defined in the following way:

$$y(t) = P.V.\int_{\partial v} v\rho^v(t,v|\eta)dv = \langle v(t,\eta)\rangle \tag{24}$$

The mean membrane potential can thus be considered as:

$$\langle v(t)\rangle = \int_{\partial\eta} y(t,\eta)\mathcal{L}(\eta)d\eta \tag{25}$$

Moreover, under the condition $v_{peak} = -v_{reset} \to \infty$, the population firing rate can be related to the Lorentzian distribution parameters:

$$r(t,\eta) = \lim_{v\to\infty} G^v(v,\langle u|\eta\rangle,\eta,M_{D1},s)\rho^v(t,v|\eta) \propto a v_{peak}^2 \cdot \frac{x(t,\eta)}{\pi v_{peak}^2} = \frac{a}{\pi}x(t,\eta) \tag{26}$$

Although this assumption is not plausible from a biological point of view, it is essential for the validity of the Lorentzian ansatz 23. In fact, it allows the passage from the QIF model to the theta neuron model [47], via the change of variable $v = tan(\theta/2)$. For the latter the ansatz 23 correspond to the OA ansatz [18, 1], used to investigate low-dimensional dynamics of large population.
By integrating over the noise we get the population firing rate:

$$r(t) = \int_{\partial\eta}\frac{a}{\pi}x(t,\eta)\mathcal{L}(\eta)d\eta \tag{27}$$

Next we proceed to substitute the Lorentzian ansatz 23 into the continuity equation 22 to obtain the time evolution for the parameters of the distribution. We obtain a second order equation in v and equating the coefficients of v^2 and v to 0, we find respectively:

$$x'(t,\eta) = 2axy + bx - x\left((M_{D1}+B_{M_{D1}})g_a s_a + g_g s_g\right) \tag{28}$$

$$y'(t,\eta) = ay^2 + by + c - ax^2 - \langle u|\eta\rangle + \eta + I_{ext} + (M_{D1}+B_{M_{D1}})g_a s_a(e_a - y) + g_g s_g(e_g - y) \tag{29}$$

Both of the results, lead to the disappearance of the coefficient related to v^0. By defining a new complex variable $z(t,\eta) = x(t,\eta) + iy(t,\eta) = \frac{\pi}{a}r(t,\eta) + i\langle v(t,\eta)\rangle$ we can write the continuity equation 22 in the form:

$$\frac{\partial}{\partial t}z = z\left(b - (M_{D1}+B_{M_{D1}})g_a s_a - g_g s_g\right) + i\left[-az^2 - \langle u|\eta\rangle + \eta + c + I_{ext} + (M_{D1}+B_{M_{D1}})g_a s_a e_a + g_g s_g e_g\right]. \tag{30}$$

Up to this point we have obtained the mean field equations for $r(t,\eta)$ and $\langle v(t,\eta)\rangle$ as functions of the intrinsic current η. In order to compute the above integrals 25 27 we assume that the heterogeneous intrinsic current η is distributed according to a Lorentzian distribution, as done in previous works [1, 2]:

$$\mathcal{L}(\eta) = \frac{1}{\pi}\frac{\Delta_\eta}{\left[\eta-\bar{\eta}\right]^2 + \Delta_\eta^2}, \tag{31}$$

with Δ_η and $\bar{\eta}$ respectively the half-width at half-maximum and the centroid of the distribution.
We stress that the choice for the distribution of the intrinsic current $\mathcal{L}(\eta)$ is arbitrary.
In particular, the Lorentzian distribution is an advantageous choice since it only has one pole in the negative plane, hence reducing the complexity of the resulting mean field system. Other distributions can be taken into account (as the Gaussian distribution), however, the final results are qualitatively similar to those obtained using the Lorentzian ansatz, as shown in [1]. In general Ott and Antonsen [18] showed that, if $\mathcal{L}(\eta)$ has n complex-conjugate pairs of pole, the resulting mean field system will be made by made by n complex-value ordinary differential equations such as 30.
By exploiting the residue theorem we can compute the complex integrals 25 and 27 obtaining:

$$\begin{aligned} r(t) &= \frac{\pi}{a} x(t, \bar{\eta} - i\Delta_\eta) \\ \langle v(t) \rangle &= y(t, \bar{\eta} - i\Delta_\eta) \end{aligned} \tag{32}$$

The complete derivation of these results is discussed in 4.2.
Substituting these results into the evolution equation for the complex variable $z(t)$ 30 we derive the mean field equations both for the average membrane potential and the population firing rate.
Finally, we consider that $\langle w \rangle = \int_{\partial\eta} \langle w|\eta \rangle \mathcal{L}(\eta) d\eta$ one may derive the final mean field reduction, which is given by:

$$\begin{cases} r(t)' = 2a\langle v \rangle r + br - r\left((M_{D1} + B_{M_{D1}}) g_a s_a + g_g s_g\right) + \frac{a\Delta_\eta}{\pi} \\ \langle v \rangle' = a\langle v \rangle^2 + b\langle v \rangle + c - \langle u \rangle + \bar{\eta} + I_{ext} + (M_{D1} + B_{M_{D1}}) g_a s_a (e_a - \langle v \rangle) + g_g s_g (e_g - \langle v \rangle) - \frac{\pi^2 r^2}{a} \\ \langle u \rangle' = \alpha(\beta\langle v \rangle - \langle u \rangle) + u_{jump} r(t) \\ s_a' = -s_a/\tau_{s_a} + s_{a,jump} r(t) \\ s_g' = -s_g/\tau_{s_g} \\ \tau_{[Dp]}[Dp]' = k c_{dopa} - \frac{V_{max}[Dp]}{K_m + [Dp]} \\ \tau_{M_{D1}} M_{D1}' = -M_{D1} + \frac{R_d}{1 + exp(S_p([Dp]+1))} \end{cases} \tag{33}$$

2.3 Numerical simulations for single spiking population

Once we derived the equations, we compare simulations realized simulating the mean field system with full network simulations to observe the validity and potential limitations of this reduction.
For the full spiking network simulations we consider $N = 2000$ spiking neurons all-to-all coupled with synaptic activity described by the single exponential model. Then we averaged at each time step the values of the neurons in the system to get $\langle v(t) \rangle$ and $\langle u(t) \rangle$.
Spiking network simulations were carried out using the Python package Brian2. It is a widely spread package which allows to perform simulations by defining the equation controlling the evolution of each single point neuron together with the synaptic connection within the population. Moreover, it automatically records useful observables as the times at which each neuron 'spikes' and the instantaneous firing rate (i.e. $r(t)$).
For the numerical simulations the Lorentzian distribution for the intrinsic current $\mathcal{L}(\eta)$ is generated using the technique of the inverse transform sampling. Thus, the i-th neuron received:

$$\eta_i = \bar{\eta} + \Delta_\eta \tan(\pi(k_i - 0.5)) \tag{34}$$

where k_i is sampled from the an uniform distribution with support on the interval (0,1).
The values for the parameters which was used can be find in Table 1. We point out that we set large positive and negative values of v_{th} and v_{reset}, which are unreasonable biologically, to mimic the approximation to theta neurons.
The results of the simulations are shown in Figure 4.
First of all, we observe that the dynamical behavior of the mean field simulations qualitatively match that of the full spiking network of neurons. However, we notice that there is a quantitative displacement between the time evolution of the complete network and that of the mean field model, as is also observed in previous works [43, 46, 3, 48, 7]. It can be mainly addressed to the finite size effect of the system of neurons together with a partial or total failure of one or more of the approximations done to derived the model. Namely,at the edges between region the condition $\langle u|v, \eta \rangle = \langle u|\eta \rangle$ could not be sufficient anymore, hence one may improve the approximation by consider higher order moment closure assumption. Nevertheless, doing so we would have to consider an higher number of equation in the mean field system, at the expense of its efficiency.
Those issues cause a "phase shift" between the space of parameters of the two different descriptions.
Afterwards, we analyse the behavior of the reduced system over different values of the parameters.

a	0.04	I_{ext}	0	k	10000
b	5	g_a	12	K_m	150
c	140	g_g	12	V_{max}	1300
α	0.013	e_a	0	R_d	1
β	0.4	e_g	-80	S_p	-1
u_{jump}	12	$s_{j,a}$	0.8	B_d	0.2
v_{th}	400	τ_{s_a}	2.6	$\tau_{[Dp]}$	500
v_{reset}	-400	τ_{s_g}	2.6	$\tau_{M_{D1}}$	500

Table 1: Values of the parameters to simulate aQIF model

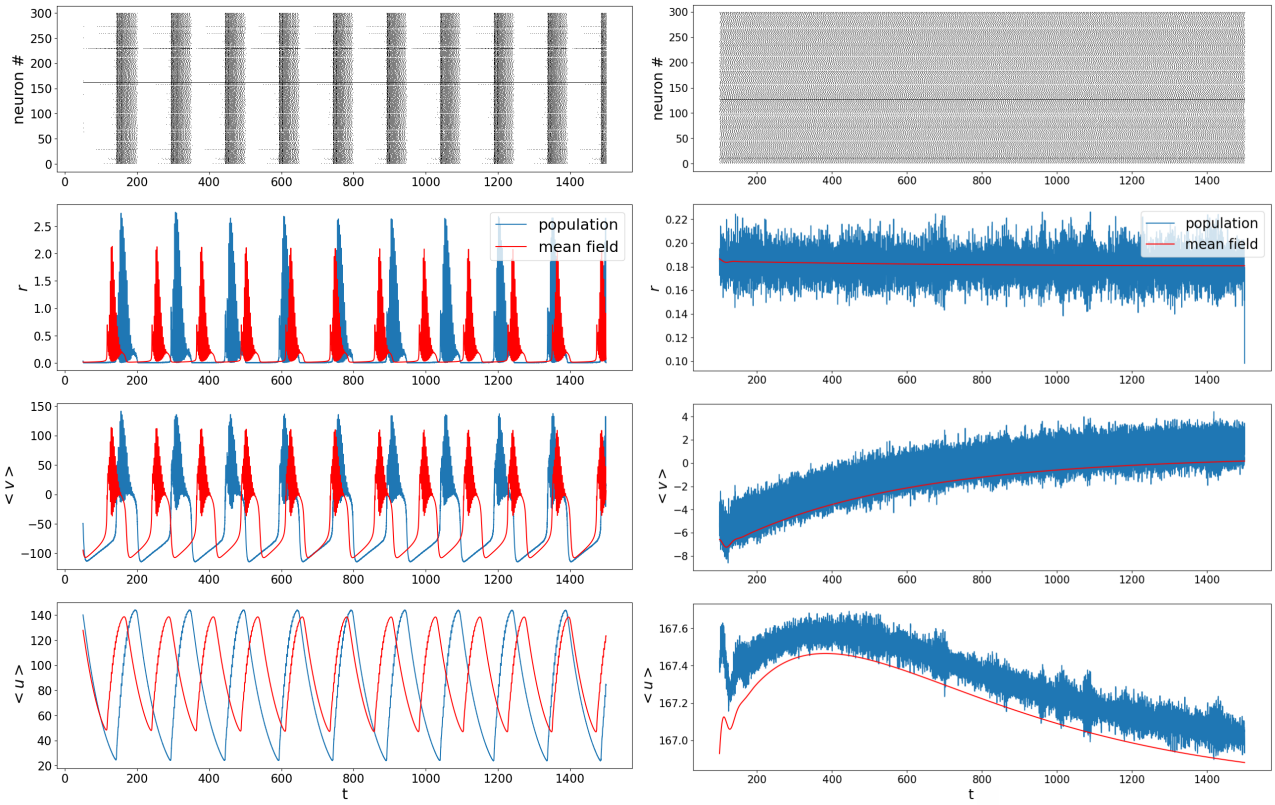

Figure 4: Comparison of the temporal behaviour of the network and the mean field simulation, with 4a $\bar{\eta} = 4.5$ and $c_{dopa} = 0.0001$ and in 4b $\bar{\eta} = 35$ and $c_{dopa} = 0.001$.
The first row shows raster plot of 300 randomly selected neurons. Each element on the y-axes corresponds to a single neuron and a black dot indicates each time the i-th neuron emits a spike.
The following rows shows respectively population firing rate, mean membrane potential and mean adaptation current both for the network (blue) and the mean field model (red). We reproduces two different dynamical regimes: bursting (4a) on the left and asynchronous spiking (4b) on the right. The mean field simulations correctly reproduce the qualitative behaviour of the spiking network in both the presented regimes.

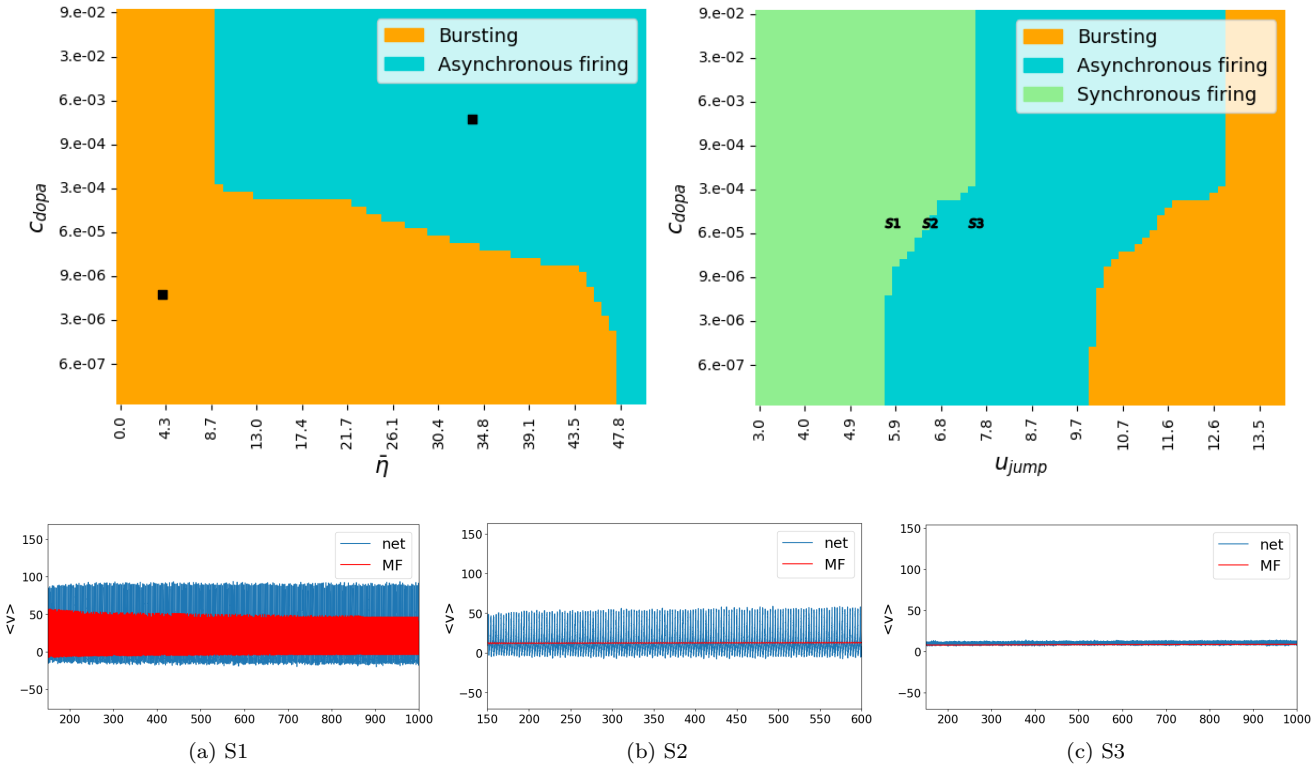

(a) S1 (b) S2 (c) S3

Figure 5: Behaviour of the mean field system for different values of relevant parameters. The figures 5a and 5b are obtained by changing progressively the values of $c_{dopa}/\bar{\eta}$ with fixed u_{jump} and c_{dopa}/u_{jump} with constant $\bar{\eta}$ respectively. The values of the others parameters are the same that in 1. The regime is identified through the analyses of the after-transient behaviour of the simulations by considering the value of the variance as distinguishing feature (row figures with the value of variance are presented in appendix 4.3).
In the second row, average membrane potential, both for mean field reduction and spiking network are presented. These plots highlight limitation of the mean field model at the shift between different regimes (synchronous and asynchronous firing in this case). For each plot the values of parameters c_{dopa} and u_{jump} is depicted in 5a. Specifically, at the boundary 5b the mean field simulations fail to capture the behaviour of the network simulations also qualitatively. In fact, we observe in 5b and 5c that slightly change in the parameter values has a relevant effect on the ability of the reduced model to capture the dynamical features of the population.

Namely, we selected three relevant ones: c_{dopa} the concentration of dopamine 7, u_{jump}, the after-spike increment of the adaptation variable 3 and $\bar{\eta}$, related to the heterogeneity term 31. Thereafter, we performed different simulations of the mean-field system sweeping over the values of the aforementioned parameters to test whether the reduction is able to reproduce how their change shapes the dynamics of the spiking network. To achieve that, we focused on the behavior of simulation once a stable regime is reached. In particular, we performed simulations for a long time (t 10000) with a really narrow time step (dt 0.001) and retained only the last 1000 time intervals to avoid transient dynamics. Hence, by computing the variance of the mean firing rate over this interval we were able to identify different dynamical regimes, presented in 5a and 5b. The figures 5a, 5b allowed us to identify three distinct regimes:

- *asynchronous firing*, when each single neuron has a distinct behaviour and there isn't any kind of synchronization between the single elements of the spiking network
- *synchronous firing*, characterized by fast synchronous firing activity
- *bursting*, which refers to patterns of neural activity consisting of episodes of relatively fast spiking separated by intervals of quiescence

Furthermore, we observed that the same regimes characterize also the spiking network. As an example, we highlight the fact that the two black dots in 5a refer to the combination of parameter values used to represent 4a and 4b.

Moreover, the reduced model also manages to capture the transition between different dynamical regimes, as we can observe in 5a and 5c.
However, the performance of the reduction is worse at the boundary between dynamical regions. We may notice in 5 that the system is more sensitive to small changes of the parameters as soon as it get closer to edges, as highlighted also in [2, 43, 46]. This particular sensitivity leads to a failure of the mean field reduction also from a qualitative point of view at the boundary of the region, as represented in 5b.

2.4 Mean field reduction for two coupled spiking networks

In the previous section we observed that the mean field reduction of the spiking network is able to reproduce qualitatively the behavior of the simulated population with robust results, at least far from the boundaries between dynamical regimes distinct areas.
In this section we would like to make a further step by considering two different population of neurons, to asses whether or not the techniques and the assumptions we made still resist.
We point out that what we are going to present can be considered more a toy model and a first attempt to take into account the interaction between the dynamics of two population of neurons under the effect of dopamine modulation. In order to obtain a more precise model we would have to clarify the type of synapses and the effect of different receptors.
A single neuron within each population can be described by the Izhikevich model at microscopic level:

$$v'_{\gamma,i} = av^2_{\gamma,i} + bv_{\gamma,i} + c - u_{\gamma,i} + I_{\gamma,ext} + I_{\gamma,syn} + \eta_{\gamma,i} \tag{35}$$
$$u'_{\gamma,i} = \alpha(\beta v_{\gamma,i} - u_{\gamma,i}) \tag{36}$$

The subscript $\gamma = E, R$ highlights whether the effect of dopamine receptors that characterize the population are enhanced or reduced by the presence of dopamine in the synaptic cleft. Precisely, the two systems are characterized by different sign for the value related to the sensitivity of the receptors S_p 6, that is negative for the "enhancing" neurons (E) and positive for the "reducing" (R) ones.
Furthermore, we also consider the two population have to have different performance for the adaptation variable due to diverse value of the after-spike increment $u_{jump,k}$ [43]. Namely, we consider population E to be adapting stronger, $u_{jump,E} = 12$ with respect to population I, $u_{jump,E} = 3$.
When membrane potential crosses the threshold (i.e an action potential is emitted) the usual reset condition applies:

$$\begin{aligned} v_{\gamma,i} \geq v_{\gamma,peak}, \text{ then } v_{\gamma,i} &\leftarrow v_{\gamma,reset} \\ u_{\gamma,i} &\leftarrow u_{\gamma,i} + u_{\gamma,jump} \end{aligned} \tag{37}$$

The two populations are connected through the synaptic current term $I_{\gamma,syn}$:

$$I_{E,syn} = J(M_E + B_{M_E})g_{EE}s_E(e_E - v_{E,i}) + (1-J)(M_R + B_{M_R})g_{RE}s_R(e_R - v_{E,i}) \tag{38}$$
$$I_{R,syn} = J(M_E + B_{M_E})g_{ER}s_E(e_E - v_{E,i}) + (1-J)(M_R + B_{M_R})g_{RR}s_R(e_R - v_{E,i}) \tag{39}$$

where g_{EE}, g_{RR} indicates the maximum synaptic conductance within the single population and g_{ER}, g_{RE} the value between the population.
The term $J = \frac{N_E}{N_E+N_R}$ represent the proportion of neurons belonging to the "enhanced" population with respect to the total number of neurons in the network. The variable s_E (s_R) represents the proportion of open synapses due to neurons in the enhanced (reduced) population. In the following, these gating variables are considered to be governed by the single exponential synapse model described before 5. Finally, e_E, e_R represent the values of the reversal potential for the two distinct populations.
With a view to obtain a mean field reduction for the two coupled spiking network, in first approximation, we consider to exploit once again the Lorentzian ansatz and the method presented previously by describing the two populations with their own distinct density function:

$$\rho_\gamma(v_\gamma, u_\gamma, \eta_\gamma) = \rho^u_\gamma(u_\gamma|v_\gamma, \eta_\gamma)\rho^v_\gamma(v_\gamma|\eta_\gamma)\mathcal{L}_\gamma(\eta_\gamma) \tag{40}$$

g_{EE}	12	$v_{reset,E}$	-300
g_{ER}	12	$v_{th,E}$	450
g_{RR}	12	$v_{reset,R}$	-300
g_{RE}	12	$v_{th,R}$	450
$u_{E,jump}$	12	$s_{jump,E}$	0.8
$u_{R,jump}$	3	$s_{jump,R}$	0.8
$I_{E,ext}$	0	$S_{p,E}$	-1.0
$I_{R,ext}$	0	$S_{p,R}$	1.0
e_E	0	J	
e_R	0		

Table 2: Values of the parameters to simulate coupled network. The values which are not present in this table are considered to be the same as 1

Moreover, by considering the Lorentzian shape both for ρ_γ^v and $\mathcal{L}_\gamma(\eta_\gamma$ as described earlier we derive the following mean field system of coupled population (the complete derivation follow the same steps that 4.2):

$$r'_E = 2av_E r_E + br_E - r_E\left(J(M_E + B_{M_E})g_{EE}s_E + (M_R + B_R)g_{RE}s_R\right) + \frac{a\Delta_{\eta,E}}{\pi} \tag{41}$$

$$v'_E = av_E^2 + bv_E + c - u_E + \bar{\eta_E} + I_{ext,E} + J(M_E + B_E)g_{EE}s_E(e_E - v_E) + \tag{42}$$

$$+ (1-J)(M_R + B_{M_R})g_{RE}s_R(e_R - v_E) - \frac{\pi^2 r_E^2}{a} \tag{43}$$

$$u'_E = \alpha(\beta v_E - u_E) + u_{E,jump}r_E \tag{44}$$

$$s'_E = -s_E/\tau_{s_E} + s_{E,jump}r_E \tag{45}$$

$$r'_R = 2av_R r_R + br_R - r_R\left(J(M_E + B_{M_E})g_{ER}s_E + (M_R + B_{M_R})g_{RR}s_R\right) + \frac{a\Delta_{\eta,R}}{\pi} \tag{46}$$

$$v'_R = av_R^2 + bv_R + c - u_R + \bar{\eta_R} + I_{ext,R} + J(M_E + B_{M_E})g_{ER}s_E(e_E - v_R) + \tag{47}$$

$$+ (1-J)(M_R + B_{M_R})g_{RR}s_R(e_R - v_R) - \frac{\pi^2 r_R^2}{a} \tag{48}$$

$$u'_R = \alpha(\beta v_R - u_R) + u_{I,jump}r_R \tag{49}$$

$$s'_R = -s_R/\tau_{s_R} + s_{R,jump}r_R \tag{50}$$

$$\tag{51}$$

In the following we analyze the dynamics of the mean-field system and examine how well it reproduces the macroscopic activities of the spiking network composed by the two populations. The parameter values can be found in 2.

Evolution in time of dopamine local concentration $[Dp]_{,k}$ and its receptors M_k, with $k = E, R$, are described by distinct equation 7 and 6 for both the population.

2.5 Numerical simulations for two coupled populations

As it was presented for the single population case, now we compare the behavior of the two coupled populations mean field reduction with the corresponding spiking networks.

Also in this case simulation for the connected spiking networks were realised using the package Brian2. The total number of neurons was set to $N = (N_E + N_R) = 3000$.

First and foremost, we observe in 6a and 6b that the mean field reduction is successfully capable of reproducing the distinct dynamical regimes of the spiking network simulation also in the case of two coupled populations. As we highlighted previously, also in this situation we can observe a quantitative mismatch between the mean field and complete network simulations which persists.

Furthermore, we observe how the behavior of the strongly adapting population E changes, by considering different values of J, hence different values for N_1 and N_2. To observe that we perform different simulation of the mean field model changing the value of J. Similarly to what we presented in for the single population analyses, for each value of J and for each couple of parameters $c_{dopa,k}/\bar{\eta_k}$ we simulated the system of equation for a time long enough to avoid transient effects. Afterward, we consider the last 1000 time units and we compute the standard deviation of the mean firing rate over this window. Results are presented in figure 6. In 6c we notice that increasing the proportion of stronger adapting neurons asynchronous behavior within the population, characterized by a low value

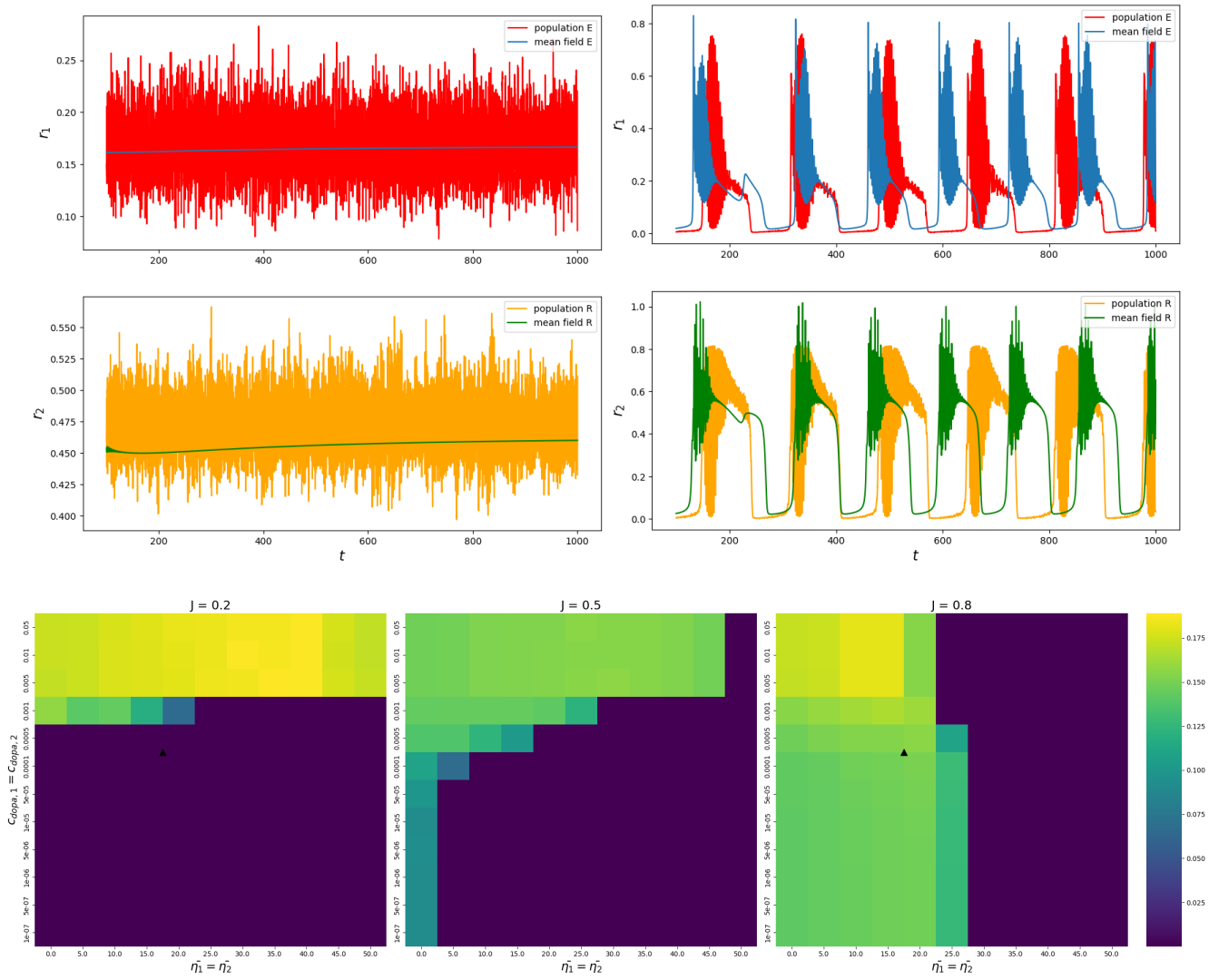

Figure 6: Comparison between mean field system and spiking network simulation for two coupled distinct population. First two rows represent direct contrast between network and mean field simulations, respectively for population E with enhancing sensitivity (top) and R with reducing sensitivity (low). As highlighted in 4a and 4b mean field reduction properly reproduces qualitative behavior of the entire coupled populations in different dynamical regimes. In last row standard deviation of mean firing rate analysis is represented for different values of J,c_{dopa} and $\bar{\eta}$. Changing the parameter affect the area of the purple zone which is characterized by low values of standard deviation, i.e. by stable behavior of the mean field system which is related to asynchronous behavior of the full system.

for the standard deviation in the mean field reduction, became less likely. This indicates that stable asynchronous behavior is more likely in a network with a lower proportion of neurons with strong adaptation. In fact, we observe that the asynchronous purple area decrease as J increase.
This result is consistent to that obtained in 5a for a single population. Indeed if we consider the evolution of firing rate and membrane potential of population E compared to that of a single population, what changes is the total synaptic current I_{syn}. Hence when J increase 6c became similar to 5a.
Furthermore, we may also monitor the different effect of dopamine modulation on the neural activity when the sensitivity of its receptor changes. In fact, changing J also affect which is the 'dominant' effect between enhancement and reduction for the receptors. In 6c, for $J = 0.2$ we observe synchronous activity within the network (characterized by higher values of standard deviation) only for relevant values of c_{dopa}, i.e. just for high concentration of dopamine.

3 Conclusion and future perspectives

In this work we derived a mean field model for a network of aQIF neurons modulated by the effect of dopamine, inspired by previous works on this topic [2, 1].
The advantage of this method lays in the capacity of reproducing qualitatively the behavior of a large population of neurons in a computationally efficient way. Thus, it allows to directly study the dynamics of the mean observables values of the network, so as to identify possibly interesting dynamical regimes for the network of coupled neurons.
The major drawback of the presented method resides in the number of assumptions which were used. However, it is certainly possible to relax some of them. As instance, the choice of the Lorentzian ansatz 31 for the distribution of the intrinsic current η is a mathematical convenience, but other distribution could be taken into account, as evinced in [1]. Also the finite-size effects encountered in the numerical simulations could be blunted by consider an higher number of neurons, in fact Chen and Campbell [2] already showed remarkable result using $N = 8000$ neurons in the network.
It would be interesting for the future to further analyze the performance of the mean field system for different values of the parameters, in order to identify more firing pattern [8].
Since the typical time scale of neuromodulator dynamics is slower than that of neuron activity, this particular method can also be easily extended by considering the dynamics of different neuromodulators together with dopamine, such as serotonin. In fact, although it is interesting to focus just on one of them at early stage to understand its effect, commonly neural circuits are modulated by a large variety of different molecules at the same time [27].
Moreover, it will be worth to apply the framework used in the presented mean field derivation could be adapted to the study of more biologically realistic models, as attempted in [3]. In fact, it would be useful to incorporate into the selected model measurable and explicit biophysical mechanism, to obtain a wider comprehension of neural dynamics.
We have shown that the mean field reduction also hold when we consider coupled spiking networks, so it could be interesting to investigate the response of neural activity coming from different brain areas under the effect of neuromodulation. In this sense, it would be interesting for future work to consider a better defined, in term of synapses and neuromodulator effect, microscopic model. Furthermore, future work would study potential dynamics emerging from the interconnection of distinct spiking network. In particular, it would be worthy to deepen the knowledge of the effect of the dopamine modulation to the population dynamics for further use the mean field equations to describe the evolution of single node at whole-brain scale [49, 50, 51].
At this level, single nodes and connection between them can also be implemented in simulated environment of The Virtual Brain (TVB) [52], to investigate how neuromodulation shapes the electrophysiological activity patterns in the human brain.
By the consideration of biophysical plausible models to obtain whole-brain network, it should also be possible to realised personalized models by properly fitting parameters with data derived by brain recordings (for instance EEG and fMRI).
Thereby, this could contribute to the understanding we have about brain functioning in healthy and altered state, facilitating the developing of ad-hoc treatment and screening strategies [53], as it already being done for epilepsy [54].
Finally, it would be attractive to compare the results obtained with the derivation presented in this work with other approaches to obtain mean field model of neuronal activity already used in literature [4, 43, 7]. This could help to identify possible common features of the different frameworks and mainly that are the areas of validity in which each of these models is better at effectively reproducing the dynamics of the population of neurons considered.
In conclusion, this mean field reduction framework provides a reliable and computationally efficient tool to investigate the dynamics of an ensemble of neurons whose activity is modulated by the presence of dopamine in the extracellular environment.

References

[1] Ernest Montbrió, Diego Pazó, and Alex Roxin. "Macroscopic Description for Networks of Spiking Neurons". In: (2015). DOI: 10.1103/PhysRevX.5.021028.

[2] Liang Chen, · Sue, and Ann Campbell. "Exact mean-field models for spiking neural networks with adaptation". In: 1 (2022), p. 3. DOI: 10.1007/s10827-022-00825-9. URL: https://doi.org/10.1007/s10827-022-00825-9.

[3] Abhirup Bandyopadhyay et al. "Mean-field approximation of network of biophysical neurons driven by conductance-based ion exchange". In: *bioRxiv* (2022). DOI: 10.1101/2021.10.29.466427. eprint: https://www.biorxiv.org/content/early/2022/12/03/2021.10.29.466427.full.pdf. URL: https://www.biorxiv.org/content/early/2022/12/03/2021.10.29.466427.

[4] Matteo di Volo et al. "Biologically Realistic Mean-Field Models of Conductance-Based Networks of Spiking Neurons with Adaptation". In: *Neural Computation* 31.4 (Apr. 2019), pp. 653–680. ISSN: 0899-7667. DOI: 10.1162/neco_a_01173. eprint: https://direct.mit.edu/neco/article-pdf/31/4/653/1050655/neco_a_01173.pdf. URL: https://doi.org/10.1162/neco%5C_a%5C_01173.

[5] Moritz Augustin et al. "Low-dimensional spike rate models derived from networks of adaptive integrate-and-fire neurons: Comparison and implementation". In: *PLOS Computational Biology* 13.6 (June 2017), pp. 1–46. DOI: 10.1371/journal.pcbi.1005545. URL: https://doi.org/10.1371/journal.pcbi.1005545.

[6] Caglar Cakan and Klaus Obermayer. "Biophysically grounded mean-field models of neural populations under electrical stimulation". In: *PLOS Computational Biology* 16.4 (Apr. 2020), pp. 1–30. DOI: 10.1371/journal.pcbi.1007822. URL: https://doi.org/10.1371/journal.pcbi.1007822.

[7] Nicolas Brunel. "Dynamics of sparsely connected networks of excitatory and inhibitory spiking neurons." In: *J Comput Neurosci.* (2000). DOI: 10.1023/a:1008925309027.

[8] E.M. Izhikevich. "Simple model of spiking neurons". In: *IEEE Transactions on Neural Networks* 14.6 (2003), pp. 1569–1572. DOI: 10.1109/TNN.2003.820440.

[9] Sergei Gepshtein et al. "Dopamine Function and the Efficiency of Human Movement". In: *Journal of Cognitive Neuroscience* 26.3 (Mar. 2014), pp. 645–657. ISSN: 0898-929X. DOI: 10.1162/jocn_a_00503. eprint: https://direct.mit.edu/jocn/article-pdf/26/3/645/1946802/jocn_a_00503.pdf. URL: https://doi.org/10.1162/jocn%5C_a%5C_00503.

[10] Mati Joshua, Avital Adler, and Hagai Bergman. "The dynamics of dopamine in control of motor behavior". In: *Current Opinion in Neurobiology* 19.6 (2009). Motor systems • Neurology of behaviour, pp. 615–620. ISSN: 0959-4388. DOI: https://doi.org/10.1016/j.conb.2009.10.001. URL: https://www.sciencedirect.com/science/article/pii/S0959438809001305.

[11] Basma Radwan, He Liu, and Dipesh Chaudhury. "The role of dopamine in mood disorders and the associated changes in circadian rhythms and sleep-wake cycle". In: *Brain Research* 1713 (2019). More than a reward molecule: The role of dopamine in aversively motivated behavior, pp. 42–51. ISSN: 0006-8993. DOI: https://doi.org/10.1016/j.brainres.2018.11.031. URL: https://www.sciencedirect.com/science/article/pii/S0006899318305973.

[12] Ryan T. LaLumiere. "5 - Dopamine and Memory". In: *Identification of Neural Markers Accompanying Memory*. Ed. by Alfredo Meneses. San Diego: Elsevier, 2014, pp. 79–94. ISBN: 978-0-12-408139-0. DOI: https://doi.org/10.1016/B978-0-12-408139-0.00005-5. URL: https://www.sciencedirect.com/science/article/pii/B9780124081390000055.

[13] Rumana Chowdhury et al. "Dopamine Modulates Episodic Memory Persistence in Old Age". In: *Journal of Neuroscience* 32.41 (2012), pp. 14193–14204. ISSN: 0270-6474. DOI: 10.1523/JNEUROSCI.1278-12.2012. eprint: https://www.jneurosci.org/content/32/41/14193.full.pdf. URL: https://www.jneurosci.org/content/32/41/14193.

[14] Martin J. Dahl et al. "The integrity of dopaminergic and noradrenergic brain regions is associated with different aspects of late-life memory performance". In: *bioRxiv* (2022). DOI: 10.1101/2022.10.12.511748. eprint: https://www.biorxiv.org/content/early/2022/10/17/2022.10.12.511748.full.pdf. URL: https://www.biorxiv.org/content/early/2022/10/17/2022.10.12.511748.

[15] Marianne O Klein et al. "Dopamine: Functions, Signaling, and Association with Neurological Diseases". In: *Cellular and molecular neurobiology* 39.1 (Jan. 2019), pp. 31–59. ISSN: 0272-4340. DOI: 10.1007/s10571-018-0632-3. URL: https://doi.org/10.1007/s10571-018-0632-3.

[16] JP Kesby et al. "Dopamine, psychosis and schizophrenia: the widening gap between basic and clinical neuroscience". In: *Translational Psychiatry* (2018). DOI: 10.1038/s41398-017-0071-9.

[17] Duane Q Nykamp and Daniel Tranchina. "A Population Density Approach That Facilitates Large-Scale Modeling of Neural Networks: Analysis and an Application to Orientation Tuning". In: *Journal of Computational Neuroscience* 8 (2000), pp. 19–50.

[18] Edward Ott and Thomas M. Antonsen. "Low dimensional behavior of large systems of globally coupled oscillators". In: *Chaos: An Interdisciplinary Journal of Nonlinear Science* 18.3 (Sept. 2008), p. 037113. ISSN: 1054-1500. DOI: 10.1063/1.2930766. eprint: https://pubs.aip.org/aip/cha/article-pdf/doi/10.1063/1.2930766/13857986/037113_1_online.pdf. URL: https://doi.org/10.1063/1.2930766.

[19] Cheng Ly and Daniel Tranchina. "Critical analysis of dimension reduction by a moment closure method in a population density approach to neural network modeling". In: *Neural computation* 19 (8 2007), pp. 2032–2092. ISSN: 0899-7667. DOI: 10.1162/NECO.2007.19.8.2032. URL: https://pubmed.ncbi.nlm.nih.gov/17571938/.

[20] A. L. Hodgkin and A. F. Huxley. "A quantitative description of membrane current and its application to conduction and excitation in nerve". In: *The Journal of Physiology* 117.4 (1952), pp. 500–544. DOI: https://doi.org/10.1113/jphysiol.1952.sp004764. eprint: https://physoc.onlinelibrary.wiley.com/doi/pdf/10.1113/jphysiol.1952.sp004764. URL: https://physoc.onlinelibrary.wiley.com/doi/abs/10.1113/jphysiol.1952.sp004764.

[21] Robin De Schepper et al. "Scaffold modelling captures the structure-function-dynamics relationship in brain microcircuits". In: *bioRxiv* (2021). DOI: 10.1101/2021.07.30.454314. eprint: https://www.biorxiv.org/content/early/2021/08/01/2021.07.30.454314.full.pdf. URL: https://www.biorxiv.org/content/early/2021/08/01/2021.07.30.454314.

[22] Robin De Schepper et al. "Scaffold modelling captures the structure-function-dynamics relationship in brain microcircuits". In: *bioRxiv* (2021). DOI: 10.1101/2021.07.30.454314. eprint: https://www.biorxiv.org/content/early/2021/08/01/2021.07.30.454314.full.pdf. URL: https://www.biorxiv.org/content/early/2021/08/01/2021.07.30.454314.

[23] Tomasz Górski, Damien Depannemaecker, and Alain Destexhe. "Conductance-Based Adaptive Exponential Integrate-and-Fire Model". In: *Neural Computation* 33.1 (Jan. 2021), pp. 41–66. ISSN: 0899-7667. DOI: 10.1162/neco_a_01342. eprint: https://direct.mit.edu/neco/article-pdf/33/1/41/1865685/neco_a_01342.pdf. URL: https://doi.org/10.1162/neco%5C_a%5C_01342.

[24] Egidio D'Angelo and Viktor Jirsa. "The quest for multiscale brain modeling". In: *Trends in Neurosciences* (2022). DOI: 10.1016/j.tins.2022.06.007.

[25] Damien Depannemaecker et al. "Modeling seizures: From single neurons to networks". In: *Seizure* 90 (2021). LASSE – 15th Anniversary of Latin American Convergent Achievements in Epileptology, pp. 4–8. ISSN: 1059-1311. DOI: https://doi.org/10.1016/j.seizure.2021.06.015. URL: https://www.sciencedirect.com/science/article/pii/S1059131121001989.

[26] Gustavo Deco et al. "The Dynamic Brain: From Spiking Neurons to Neural Masses and Cortical Fields". In: *PLOS Computational Biology* 4.8 (Aug. 2008), pp. 1–35. DOI: 10.1371/journal.pcbi.1000092. URL: https://doi.org/10.1371/journal.pcbi.1000092.

[27] Eve Marder. "Neuromodulation of Neuronal Circuits: Back to the Future". In: *Neuron* 76.1 (2012), pp. 1–11. ISSN: 0896-6273. DOI: https://doi.org/10.1016/j.neuron.2012.09.010. URL: https://www.sciencedirect.com/science/article/pii/S0896627312008173.

[28] Elliot S. Krames et al. "Chapter 1 - What Is Neuromodulation?" In: *Neuromodulation*. Ed. by Elliot S. Krames, P. Hunter Peckham, and Ali R. Rezai. San Diego: Academic Press, 2009, pp. 3–8. ISBN: 978-0-12-374248-3. DOI: https://doi.org/10.1016/B978-0-12-374248-3.00002-1. URL: https://www.sciencedirect.com/science/article/pii/B9780123742483000021.

[29] Peter A. Tass. "A model of desynchronizing deep brain stimulation with a demand-controlled coordinated reset of neural subpopulations". In: *Biological Cybernetics* 89.2 (2003), pp. 81–88. ISSN: 03401200. DOI: 10.1007/s00422-003-0425-7.

[30] Martin Ebert, Christian Hauptmann, and Peter A. Tass. "Coordinated reset stimulation in a large-scale model of the STN-GPE circuit". In: *Frontiers in Computational Neuroscience* 8.NOV (2014), pp. 1–20. ISSN: 16625188. DOI: 10.3389/fncom.2014.00154.

[31] Bomin Sun et al. "Chapter 57 - Surgical Treatment for Refractory Drug Addictions". In: *Neuromodulation*. Ed. by Elliot S. Krames, P. Hunter Peckham, and Ali R. Rezai. San Diego: Academic Press, 2009, pp. 703–709. ISBN: 978-0-12-374248-3. DOI: https://doi.org/10.1016/B978-0-12-374248-3.00058-6. URL: https://www.sciencedirect.com/science/article/pii/B9780123742483000586.

[32] Ashwini D. Sharan and Ali Rezai. "Introduction". In: *Neuromodulation*. Ed. by Elliot S. Krames, P. Hunter Peckham, and Ali R. Rezai. San Diego: Academic Press, 2009, pp. 617–618. ISBN: 978-0-12-374248-3. DOI: https://doi.org/10.1016/B978-0-12-374248-3.00130-0. URL: https://www.sciencedirect.com/science/article/pii/B9780123742483001300.

[33] Benjamin D. Greenberg. "Chapter 56 - Deep Brain Stimulation for Highly Refractory Depression". In: *Neuromodulation*. Ed. by Elliot S. Krames, P. Hunter Peckham, and Ali R. Rezai. San Diego: Academic Press, 2009, pp. 689–701. ISBN: 978-0-12-374248-3. DOI: https://doi.org/10.1016/B978-0-12-374248-3.00057-4. URL: https://www.sciencedirect.com/science/article/pii/B9780123742483000574.

[34] Allen R. Dyer and Mary Pat Aardrup. "Chapter 3 - Neuromodulation Technologies: Whom Do We Serve?" In: *Neuromodulation*. Ed. by Elliot S. Krames, P. Hunter Peckham, and Ali R. Rezai. San Diego: Academic Press, 2009, pp. 21–27. ISBN: 978-0-12-374248-3. DOI: https://doi.org/10.1016/B978-0-12-374248-3.00004-5. URL: https://www.sciencedirect.com/science/article/pii/B9780123742483000045.

[35] KATHLEEN DUNLAP and GERALD D. FISCHBACH. "Neurotransmitters decrease the calcium component of sensory neurone action potentials". In: *Nature* (1978). URL: https://doi.org/10.1038/276837a0.

[36] Evan Weiss, Michael Kann, and Qi Wang. "Neuromodulation of Neural Oscillations in Health and Disease". In: *Biology* 12.3 (Feb. 2023), p. 371. ISSN: 2079-7737. DOI: 10.3390/biology12030371. URL: http://dx.doi.org/10.3390/biology12030371.

[37] Janita Turchi et al. "The Basal Forebrain Regulates Global Resting-State fMRI Fluctuations". In: *Neuron* 97.4 (Feb. 2018), 940–952.e4. ISSN: 0896-6273. DOI: 10.1016/j.neuron.2018.01.032. URL: http://dx.doi.org/10.1016/j.neuron.2018.01.032.

[38] Kate Z. Peters, Joseph F. Cheer, and Raffaella Tonini. "Modulating the Neuromodulators: Dopamine, Serotonin, and the Endocannabinoid System". In: *Trends in Neurosciences* (2021). DOI: 10.1016/j.tins.2021.02.001.

[39] Mitchell F. Roitman et al. "Dopamine Operates as a Subsecond Modulator of Food Seeking". In: *Journal of Neuroscience* 24.6 (2004), pp. 1265–1271. ISSN: 0270-6474. DOI: 10.1523/JNEUROSCI.3823-03.2004. eprint: https://www.jneurosci.org/content/24/6/1265.full.pdf. URL: https://www.jneurosci.org/content/24/6/1265.

[40] Wolfram Schultz. "Multiple dopamine functions at different time courses". In: *Annu. Rev. Neurosci.* 30 (2007), pp. 259–288.

[41] Marianne O. Klein et al. "Dopamine: Functions, Signaling, and Association with Neurological Diseases". In: *Cellular and Molecular Neurobiology* 39.1 (Nov. 2018), pp. 31–59. ISSN: 1573-6830. DOI: 10.1007/s10571-018-0632-3. URL: http://dx.doi.org/10.1007/s10571-018-0632-3.

[42] Mario Lavanga et al. "The virtual aging brain: Causal inference supports interhemispheric dedifferentiation in healthy aging". In: *NeuroImage* 283 (2023), p. 120403.

[43] Wilten Nicola and Sue Ann Campbell. "Bifurcations of large networks of two-dimensional integrate and fire neurons". In: *Journal of Computational Neuroscience* 35 (1 Feb. 2013), pp. 87–108. ISSN: 15736873. URL: https://link.springer.com/article/10.1007/s10827-013-0442-z.

[44] Morten L. Kringelbach et al. "Dynamic coupling of whole-brain neuronal and neurotransmitter systems". In: *Proceedings of the National Academy of Sciences* 117.17 (2020), pp. 9566–9576. DOI: 10.1073/pnas.1921475117. eprint: https://www.pnas.org/doi/pdf/10.1073/pnas.1921475117. URL: https://www.pnas.org/doi/abs/10.1073/pnas.1921475117.

[45] Cheng Ly Felix Apfaltrer and Daniel Tranchina. "Population density methods for stochastic neurons with realistic synaptic kinetics: Firing rate dynamics and fast computational methods". In: *Network: Computation in Neural Systems* 17.4 (2006). PMID: 17162461, pp. 373–418. DOI: 10.1080/09548980601069787. eprint: https://doi.org/10.1080/09548980601069787. URL: https://doi.org/10.1080/09548980601069787.

[46] Wilten Nicola and Sue Ann Campbell. "Mean-field models for heterogeneous networks of two-dimensional integrate and fire neurons". In: *Frontiers in Computational Neuroscience* 7 (DEC Dec. 2013), p. 68703. ISSN: 16625188. DOI: 10.3389/fncom.2013.00184. URL: https://www.ncbi.nlm.nih.gov/pmc/articles/PMC3873638/.

[47] G. B. Ermentrout and N. Kopell. "Parabolic Bursting in an Excitable System Coupled with a Slow Oscillation". In: *SIAM Journal on Applied Mathematics* 46.2 (1986), pp. 233–253. DOI: 10.1137/0146017. eprint: https://doi.org/10.1137/0146017. URL: https://doi.org/10.1137/0146017.

[48] Spase Petkoski and Aneta Stefanovska. "Kuramoto model with time-varying parameters". In: *PHYSICAL REVIEW E* 86 (2012), p. 46212. DOI: 10.1103/PhysRevE.86.046212.

[49] V.K. Jirsa et al. "The Virtual Epileptic Patient: Individualized whole-brain models of epilepsy spread". In: *NeuroImage* 145 (2017). Individual Subject Prediction, pp. 377–388. ISSN: 1053-8119. DOI: https://doi.org/10.1016/j.neuroimage.2016.04.049. URL: https://www.sciencedirect.com/science/article/pii/S1053811916300891.

[50] Rodrigo Cofré et al. "Whole-Brain Models to Explore Altered States of Consciousness from the Bottom Up". In: *Brain Sciences* 10.9 (2020). ISSN: 2076-3425. DOI: 10.3390/brainsci10090626. URL: https://www.mdpi.com/2076-3425/10/9/626.

[51] Anagh Pathak, Dipanjan Roy, and Arpan Banerjee. "Whole-Brain Network Models: From Physics to Bedside". In: *Frontiers in Computational Neuroscience* 16 (2022). ISSN: 1662-5188. DOI: 10.3389/fncom.2022.866517. URL: https://www.frontiersin.org/articles/10.3389/fncom.2022.866517.

[52] Paula Sanz-Leon et al. "Mathematical framework for large-scale brain network modeling in The Virtual Brain". In: *Neuroimage* 111 (2015), pp. 385–430.

[53] Huifang E Wang et al. "Virtual brain twins: from basic neuroscience to clinical use". In: *National Science Review* 11 (5 Apr. 2024). ISSN: 2095-5138. DOI: 10.1093/nsr/nwae079. URL: https://academic.oup.com/nsr/article/doi/10.1093/nsr/nwae079/7616087.

[54] Damien Depannemaecker et al. "From phenomenological to biophysical models of seizures". In: *Neurobiology of Disease* 182 (June 2023), p. 106131. DOI: 10.1016/j.nbd.2023.106131. URL: https://doi.org/10.1016/j.nbd.2023.106131.

[55] Wulfram Gerstner and Werner M Kistler. *Spiking neuron models: Single neurons, populations, plasticity*. Cambridge university press, 2002.

4 Supplementary material

4.1 Appendix A: Derivation of equation 5

Consider the single exponential synapse model we used for the excitatory synapse 5. Here we demonstrate that, considering $N \to \infty$:

$$s_a' = -s_a/\tau_{s_a} + \frac{s_{j,a}}{N}\sum_{i=1}^{N}\sum_{t_i^k<t}\delta(t-t_i^k) = -s_a/\tau_{s_a} + s_{j,a}j(t) = -s_a/\tau_{s_a} + s_{j,a}r(t)$$

where we highlight the contribute:

$$j(t) = \frac{1}{N}\sum_{i=1}^{N}\sum_{t_i^k<t}\delta(t-t_i^k)$$

First, let us define $n_i(t)$ the number of spikes fired by the i-th neuron in $[0,t]$. Its average value across all the network will be [55]:

$$\langle n_i(t)\rangle = \lim_{N\to\infty}\frac{1}{N}\sum_{i=0}^{N}\int_0^t\sum_{x_i^k<t}\delta(x-x_i^k)dx = \lim_{N\to\infty}\int_0^t j(x)dx$$

Next, we can define the population firing rate as:

$$r(t) = \lim_{\Delta t\to 0}\frac{1}{\Delta t}\lim_{N\to\infty}\frac{1}{N}\sum_{i=1}^{N}\frac{n_i(t+\Delta t)-n_i(t)}{N}$$

Finally, taking the limit $N\to\infty$ the previous equation can be rearranged as:

$$r(t) = \lim_{\Delta t\to 0}\frac{\langle n_i(t+\Delta t)\rangle - \langle n_i(t)\rangle}{\Delta t} = \frac{d}{dt}\langle n_i(t)\rangle$$

where the last term can be replaced by $j(t)$ in the thermodynamic limit, as shown before.

4.2 Appendix B: Derivation of the integrals 27, 25 using the residue theorem

In this section we further explain the computation of the integrals 27, 25.
Let us consider the integral:

$$\oint_{\Gamma_R} f(\eta)d\eta = \int_{-R}^{R} f(\eta)d\eta + \int_{\gamma_R} f(\eta)d\eta$$

where Γ_R is an oriented rectifiable curve and γ_R is the semicircle centered at the origin and connecting -R to R through the negative part of the imaginary plane.
Now assume:

$$f(\eta) = \frac{a}{\pi}x(\eta,t)\cdot\mathcal{L}(\eta) = \frac{a}{\pi^2}x(\eta,t)\cdot\frac{\Delta_\eta}{[\eta-\bar\eta]^2+\Delta_\eta^2} =$$
$$= \frac{a}{\pi^2}x(\eta,t)\cdot\frac{1}{2i}\left(\frac{A}{\eta-(\bar\eta-i\Delta_\eta)} - \frac{B}{\eta-(\bar\eta-i\Delta_\eta)}\right) = \frac{a}{\pi^2}x(\eta,t)\cdot\frac{1}{2i}\left(\frac{A}{\eta-\eta_1} - \frac{B}{\eta-\eta_2}\right)$$

Using the residue theorem one would get:

$$\oint_{\Gamma_R} f(\eta)d\eta = -2\pi i\cdot Res_{\eta=\eta_2}f(\eta) = \frac{a}{\pi}x(\bar\eta-i\Delta_\eta,t)$$

To recover the result we are looking for we use the Jordan lemma to demonstrate that indeed $\int_{\gamma_R} f(\eta)d\eta \to 0$ as $R\to\infty$.
First, from the ML inequality we obtain:

$$\left|\int_{\gamma_R} f(\eta)d\eta\right| = \left|\int_{\gamma_R}\frac{a}{\pi^2}x(\eta,t)\frac{\Delta_\eta}{(\eta-\bar\eta)^2+\Delta_\eta^2}d\eta\right| \le l_{\gamma_R}\cdot\sup_{\gamma_R}\left|\frac{a}{\pi^2}x(\eta,t)\frac{\Delta_\eta}{(\eta-\bar\eta)^2+\Delta_\eta^2}\right|,$$

with $l_{\gamma_R} = \frac{1}{2}(2\pi R) = \pi R$.
Next, we exploit the triangular inequality to deal with the second part of the last equation:

$$(\eta - \bar{\eta})^2 = \left|(\eta - \bar{\eta})^2\right| = \left|(\eta - \bar{\eta})^2 + \Delta_\eta^2 - \Delta_\eta^2\right| \leq \left[(\eta - \bar{\eta})^2 - \Delta_\eta^2\right] + \Delta_\eta^2.$$

Using the above relation and letting $\eta \to \pm\infty$,i.e. when we extend the radius $R \to \infty$, we obtain:

$$\left|\frac{1}{(\eta - \bar{\eta})^2 + \Delta_\eta^2}\right| \leq \frac{1}{|\eta - \bar{\eta}| - \Delta_\eta^2} = \frac{1}{R^2 - \Delta_\eta^2}.$$

Moreover, we make the reasonable assumption that the half-width at half-maximum $x(\eta, t)$ is bounded by an upper value M. As a result:

$$\left|\frac{a}{\pi^2} x(\eta, t) \frac{\Delta_\eta}{(\eta - \bar{\eta})^2 + \Delta_\eta^2}\right| \leq M \frac{a\Delta_\eta}{\pi^2} \frac{1}{R^2 - \Delta_\eta^2}.$$

Finally, putting together all the previous results

$$\lim_{R \to +\infty} l_{\gamma_R} \cdot \sup_{\Gamma_R} \left|\frac{a}{\pi^2} x(\eta, t) \frac{\Delta_\eta}{(\eta - \bar{\eta})^2 + \Delta_\eta^2}\right| = \lim_{R \to +\infty} \pi R M \frac{a\Delta_\eta}{\pi^2} \frac{1}{R^2 - \Delta_\eta^2} = 0$$

This demonstrate that indeed that the integral computed over the semicircle γ_R approaches 0 when $R \to \infty$, hence:

$$r(t) = \oint_{\Gamma_R} f(\eta) d\eta = \int_{-\infty}^{\infty} f(\eta) d\eta = \frac{a}{\pi} x(\bar{\eta} - i\Delta_\eta, t)$$

Exploiting a similar derivation we can also see that:

$$\langle v(t) \rangle = \int_{-\infty}^{\infty} y(\eta, t) \mathcal{L}(\eta) d\eta = y(\bar{\eta} - i\Delta_\eta, t)$$

4.3 Appendix C: Firing rate variance raw plots

In this section we are gonna present the raw results for the variance analyses that allowed us to obtain the figure 5a and 5b. Those figures were obtained following the procedure presented in 2.3, namely we simulated mean firing

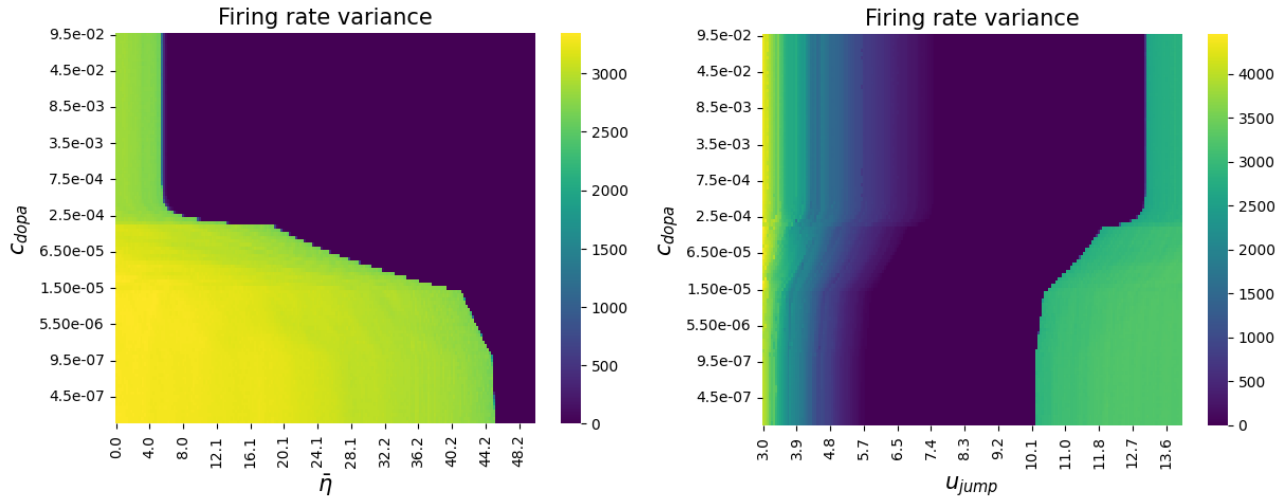

Figure 7

rate for long a really long time span to avoid transient effect and then we computed the variance over the last 1000 time step.
After that we set a threshold on the values of the variance to distinguish between the different dynamical regimes. We point out that in that case the results were supported by the study of the computational study of the system by using bifurcation analyses and numerical continuation.